Terrestrial temperature evolution of southern Africa during the Late Pleistocene and Holocene: evidence from the Mfabeni Peatland

Susanne Fietz[a*], Andrea Baker[a], Charlotte S. Miller[b], B. David A. Naafs[c], Francien Peterse[d], Jemma Finch[e], Marc Humphries[f], Enno Schefuß[b], Alakendra N. Roychoudhury[a], and Joyanto Routh[g]

[a]Department of Earth Sciences, Stellenbosch University, Stellenbosch, South Africa
[b]MARUM - Center for Marine Environmental Sciences, University of Bremen, Bremen, Germany
[c]Organic Geochemistry Unit, School of Chemistry, School of Earth Sciences, University of Bristol, Bristol, United Kingdom
[d]Department of Earth Sciences, Utrecht University, Utrecht, the Netherlands
[e]School of Agriculture, Earth and Environmental Sciences, University of KwaZulu Natal, Pietermaritzburg, South Africa
[f]School of Chemistry, University of the Witwatersrand, Johannesburg, South Africa
[g]Department of Thematic Studies - Environmental Change, Linköping University, Linköping, Sweden

*corresponding author: sfietz@sun.ac.za

Abstract

The scarcity of suitable high-resolution archives, such as ancient natural lakes, that span beyond the Holocene, hinders long-term late Quaternary temperature reconstructions in southern Africa. Here we target two cores from Mfabeni Peatland, one of the few long continuous terrestrial archives in South Africa that reaches into the Pleistocene, to generate a composite temperature record spanning the last ~43 kyr. The Mfabeni Peatland has previously been proven suitable for temperature and hydrological reconstructions based on pollen and geochemical proxies. Here we use branched glycerol dialkyl glycerol tetraethers (brGDGTs) preserved in the Mfabeni peatland to derive a new quantitative air temperature record for south-east Africa. Our temperature record generally follows global trends in temperature and atmospheric CO_2 concentrations, but is decoupled at times. Annual air temperatures during Marine Isotope Stage (MIS) 3 were moderately high (*c.* 20.5 °C), but dropped by *c.* 5 °C during the Last Glacial Maximum, reaching a minimum at *c.*16-15 ka. Asynchronous with local insolation, this cooling may have resulted from reduced sea surface temperatures linked to a northward shift in the Southern Hemisphere westerly winds. Concurrent with the southward retreat of the westerlies, and increasing sea surface temperatures offshore, warming from minimum temperatures (*c.* 15.0 °C) to average Holocene temperatures (*c.* 20.0 °C) occurred across the deglaciation. This warming was briefly but prominently interrupted by a millennial-scale cooling event of *c.* 3 °C at *c.* 2.4 ka, concurrent with a sudden change in hydrological conditions. The average Holocene temperatures of *c.* 20.0 °C were similar to those reconstructed for MIS 3, but after the 2.4 ka cooling period, air temperatures in the Mfabeni peat recovered and steadily increased towards the present. In summary, our record demonstrates that land temperature in eastern South Africa is highly sensitive to global drivers as well as nearby sea surface temperatures.

1. Introduction

Knowledge of past changes in climate is important to quantify Earth's sensitivity to carbon cycle perturbations (Seddon et al., 2016). However, although past changes in marine temperatures are relatively well constrained, much less quantitative temperature data are available for the terrestrial realm. Accordingly, one of the largest uncertainties in predicting the impact of anthropogenic climate change is the response of the terrestrial realm (Meir et al., 2006; Carvalhais et al., 2014). In particular, correctly quantifying the sensitivity of terrestrial climate to natural or anthropogenic climate forcings provides a major challenge for the paleoclimate community (Knight and Harrison, 2012). Hence, we need robust temperature reconstructions from terrestrial ecosystems to test climate model simulations of past greenhouse periods (Huber and Caballero, 2011).

In this context, reconstructing climate in southern African is of interest as it is affected by a complex interplay of driving systems and because livelihoods in southern Africa are strongly affected by a changing climate. The region currently experiences *c.* 0.4 °C warming per decade (Davis-Reddy and Vincent 2017), about twice the global average (Engelbrecht et al., 2015; Engelbrecht and Monteiro 2021). The IPCC projects further warming in south-east Africa with high confidence, such as a near-term (2021-2040) 1.6 °C increase under the SSP1-2.6, a scenario of severely cut near-future global CO_2 emissions (Gutiérrez et al., 2021: Iturbide et al., 2021). There is, therefore, an urgent scientific interest in better understanding the climate dynamics and controlling factors at various time-scales to support mitigation and adaptation strategies. Gasse et al. (2008) present a comprehensive overview of major contemporary African climates dynamics including zonal and regional characteristics, highlighting differences between regions north and south of the equator and a marked west-east asymmetry. Of particular interest for contemporary climate in south-east Africa is the warm Agulhas current and Indian Ocean to the east, the Intertropical Convergence Zone (ITCZ) to the north, and the Southern Ocean and westerlies to the south. In this context, south-east African archives record spatially and temporally heterogenous responses to climate drivers during the late Quaternary (e.g., Schmidt et al., 2014; Singarayer and Burrough, 2015; Scott and Neumann 2018; Miller et al., 2020) that likely differed between glacial and interglacial periods (e.g., Chevalier and Chase 2015; Simon et al., 2015; Hahn et al., 2021a).

Much more information has been gathered on the controls of hydroclimate than quantitative temperature variability in south-east Africa (Chevalier et al., 2020). However, temperature and hydrology are not necessarily linked. For example, local insolation has been suggested as a major driver for some hydroclimate in south-east Africa (Partridge et al., 1997), while mean annual temperatures in the region do not seem to follow local summer insolation (Chevalier and Chase, 2015). On glacial-interglacial time scales a coupling of south-eastern African hydroclimate and vegetation with Agulhas sea surface temperatures (SSTs) has also been inferred from proxy records (Dupont et al., 2011; Schmidt et al., 2014; Caley et al. 2018; Hahn et al., 2021a). A similar terrestrial to sea surface temperature relationship has been proposed for the past glacial-interglacial cycle (Truc et al., 2013; Chevalier and Chase, 2015). It is possible that the hydroclimate follows precession (insolation) forcing in some south-east African areas and West Indian Ocean sea surface temperatures in others (Neuman et al., 2014; Simon et al., 2015), while temperatures predominantly follow SSTs. However, hydroclimate in the region is also inferred to be driven by the interplay of tropical and subtropical atmospheric processes, as well as the position of the westerly winds due to changes in Southern Ocean sea ice extent (e.g., Miller et al., 2019, 2020; Hahn et al., 2021a, 2021b). This suggested interplay is consistent with dynamics affecting south, south-west and interior South Africa (Chase and Meadows 2007; Gasse et al. 2008; Stager et al., 2012; Chase et al. 2013, 2015a). Similarly, on longer-term scales, temperature in south-east African is also influenced by glacial and CO_2 feedback controls (Chevalier et al., 2020). But in addition, some records indicate a connection with Northern Hemisphere climate change (Hahn et al., 2021a, 2021b) and the impact of abrupt changes during Greenland stadials and associated changes in East Asian Monsoon intensity (Simon et al., 2015). This is similar to hydroclimate records found in south-western Africa (Chase et al., 2010), equatorial east Africa (Johnson et al., 2002; Tierney et al., 2008), and south-eastern Africa (Schefuß et al., 2011). These records illustrate the large variability in the proposed control of south-east South African temperature and hydroclimate during the late Quaternary.

A major obstacle in understanding past climate and environmental variations in southern Africa is the scarcity of continuous terrestrial archives (Scott et al., 2008; Nash and Meadows, 2012). This is partly due to the semi-arid climate that often prevents continuous records of traditional proxies, such as pollen (Chase and Meadows, 2007), to be preserved, as well as to a scarcity of lake records that span beyond the late Holocene. As an alternative to long-term lacustrine and coastal marine records, sedimentological proxy records have been generated in southern Africa's dry interior, e.g., in alluvial paleosols (Lyons et al., 2014) and pans (Lukich et al., 2020). Rock hyrax middens provided further fundamental insights into primarily south-west African terrestrial paleoclimate, using pollen- (e.g., Lim et al., 2016; Scott et al., 2018) and isotope-based reconstructions (e.g., Chase et al. 2015b, 2017, 2020). In addition, geochemical proxies, primarily $\delta^{18}O$ and $\delta^{13}C$, have previously been employed in examining southern African speleothems to reconstruct temperature and precipitation, for example, in the Cango Caves (Talma and Vogel, 1992), Cold Air Cave (Repinski et al., 1999; Stevenson et al., 1999; Holmgren et al., 2003), and Wolkberg Cave (Holzkämper et al., 2009). However, cave records can be discontinuous, and deconvolving temperature from speleothem $\delta^{18}O$ and $\delta^{13}C$ is challenging because these proxies are affected by factors other than temperature (Lachniet et al., 2009).

Peat deposits provide another form of continuous terrestrial archives as they are formed by the long-term accumulation of organic matter under waterlogged conditions, facilitating excellent preservation of organic matter (e.g., Lappalainen 2006; Yu et al., 2010; Rydin and Jeglum, 2013; Müller and Joos, 2020). Unfortunately, peatlands do not frequently form under the semi-arid conditions that prevail in southern Africa, but there are a few notable exceptions such as the Mfabeni Peatland. Mfabeni is purported to be one of the oldest continuous sedimentary archives of its kind in Africa (Finch and Hill, 2008; Grundling et al., 2013) with a basal age of *c.* 45 cal kyr BP (Baker et al., 2014). Previous studies on Mfabeni include hydrological (Clulow et al., 2012; Grundling et al., 2015) and geomorphological (Grundling et al., 2013; Humphries et al., 2017) investigations, as well as palynological (Finch and Hill, 2008) and geochemical studies including $\delta^{13}C$, $\delta^{15}N$ (Baker et al., 2014), *n*-

alkane, *n*-alkanoic acid and *n*-alkanol biomarkers (Baker et al., 2016) and leaf wax isotopes (Baker et al. 2017, Miller et al., 2019). These studies provide a valuable paleo-environmental context for this region. Temperature evolution has also been inferred from the palynological records (Finch and Hill, 2008), but pollen-based temperature reconstructions in Mfabeni suffer from a low taxonomic resolution, resulting in a low number of climate sensitive pollen-types (Chevalier and Chase, 2015).

We here use a lipid biomarker approach to reconstruct a continuous record of air temperatures using branched glycerol dialkyl glycerol tetraethers (brGDGTs) preserved in the Mfabeni peatland. BrGDGTs are produced by bacteria (Weijers et al., 2006, Sinninghe Damsté et al., 2018; Halamka et al. 2021) that are thought to adapt the molecular structure of their cell membranes in response to changing environmental conditions, especially air temperature (Weijers et al., 2007, Naafs et al. 2021). Hence, downcore changes in brGDGT distributions can be translated into temperature records using depositional setting-specific transfer functions (e.g., Weijers et al., 2007b; Peterse et al., 2012; De Jonge et al., 2014; Dearing Crampton-Flood et al., 2020; as well as Naafs et al., 2017 specifically for peats). These have been used to reconstruct past air temperatures for various environments and geological time intervals, including peats (e.g., Ballantyne et al., 2010; Weijers et al., 2011a; Zheng et al., 2015, 2017). We apply the peat-specific temperature calibration ($MAAT_{peat}$; Naafs et al., 2017) to two individual Mfabeni peat cores to generate a combined, continuous, quantitative air temperature record for south-east Africa spanning the past *c.* 43 kyr. We use two cores retrieved from sites approximately 1 km apart to derive a stacked record minimizing site-specific variability. We furthermore assess the potential presence of a seasonal bias and an impact of shifts in the peatland's water table on the reconstructed temperatures. Finally, we place the timing and direction of trends in our stacked Mfabeni air temperature record in a southern African and global climatic context.

2. Methods

2.1. Site description and sampling

Mfabeni Peatland (*c.* 28.1 °S; 32.5 °E) is located within an interdunal basin (Botha and Porat, 2007) on the eastern shores of Lake St Lucia, the main landmark of the UNESCO World Heritage iSimangaliso Wetland Park in northern KwaZulu Natal, South Africa (Figure 1). The peatland formed as part of the greater Natal Mire Complex via valley infilling within the KwaMbonambi formation coastal dune depression (Smuts, 1992). The area falls within a sub-tropical climatic zone, with approximately 80% of the annual rainfall (900 – 1200 mm) occurring during the austral summer months (Grundling, 2001; Taylor et al., 2006a; Clulow et al., 2012). Modern-day mean monthly temperature ranges between *c.* 18 °C (July) and 25 °C (January), and the annual average air temperature is *c.* 21.5 °C.

The north-south aligned 10 m thick Mfabeni peat deposit (Grundling et al., 2013) has a surface extent of 30 km^2 (Clulow et al., 2012). Despite the coastal location, Mfabeni is a groundwater fed system. The hydrology of the peatland is dominated by groundwater recharge from the Maputaland aquifer and local precipitation (Taylor et al., 2006b; Grundling et al., 2013). Sea level changes occurred since peat accumulation began in the Mfabeni Mire. During the Pleistocene, i.e. during Marine Isotope Stage (MIS) 3, the sea level was c. 40-60 m lower than present (Ramsay and Cooper, 2001). Sea levels dropped to 125 m below current levels during MIS 2 (LGM, *c.* 18 ka) but increased thereafter to reach present levels by *c.* 6.5 ka (Grundling, 2013, Ramsay and Cooper 2001). Persistent groundwater input from the Maputaland aquifer coupled with local precipitation resulted in continuous, but variable rates of peat accumulation (Baker et al., 2014, 2016). Throughout this time, the adjacent *c.* 55 kyr old coastal dune barrier (Porat and Botha, 2008) purportedly protected the coastal Mfabeni basin from sea level transgression and erosion (Grundling et al., 2013). In addition, a clay layer may have prevented water losses at times of low sea level (Grundling et al., 2013). Pollen records throughout this time, particularly the occurrence of *Typha*, indicate freshwater conditions in the Mfabeni Basin (Grundling et al., 2013).

The vegetation composition of the peatland can be broadly divided into swamp forest at the western margin of the site, with the remainder comprising open reed-sedge dominated communities typified by, *inter alia*, Cyperaceae spp., *Typha capensis*, *Sphagnum truncatum*, *Xyris natalensis,* and *Restio zuluensis* (Venter, 2003). Venter (2003) performed a detailed vegetation classification of the site, dividing the swamp forest communities as follows: *Syzygium cordatum*-*Stenochlaena tenuifolia*, *Ficus trichopoda*-*Nephrolepis biserrata,* and *Barringtonia racemosa*-*Bridelia micrantha*.

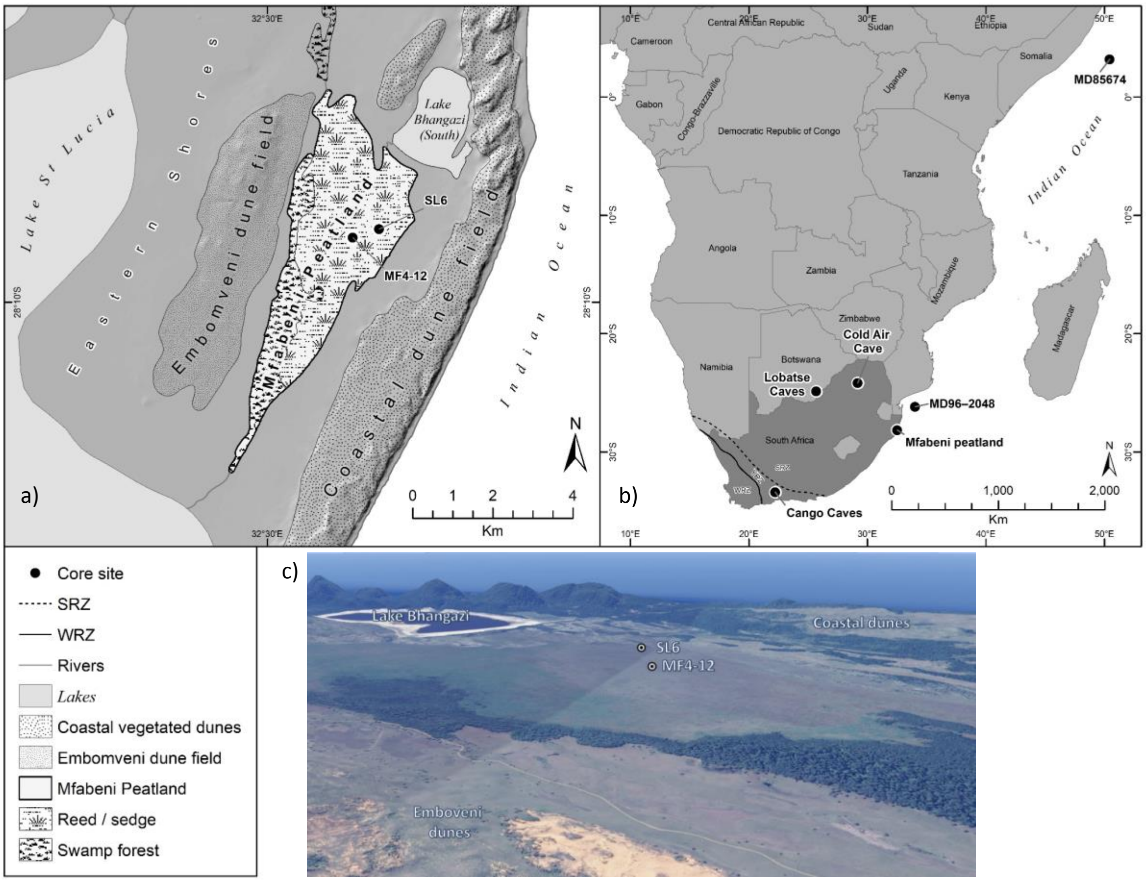

Figure 1*: (a) Geomorphological site map of Mfabeni Peatland indicating the locations of core SL6 and MF4-12, adapted from Miller et al., 2019, (b) Location of Mfabeni Peatland and records referred to in this study. (c) Google Earth image showing the position of the Mfabeni Peatland and coring locations in an interdunal valley, adapted from Humphries et al. (2017). WRZ - Winter Rainfall Zone, YRZ - Year-round Rainfall Zone, SRZ - Summer Rainfall Zone (Chase and Meadows, 2007).*

Two independently retrieved Mfabeni cores were utilized in this study. The longer (810 cm) core SL6 was extracted from the deepest part of the peatland in June 2011 (28.15021 °S; 32.52508 °E) using a Russian peat corer with a sampling barrel measuring 5 cm x 50 cm. The second, slightly shorter core MF4-12 (696 cm, corrected for compaction to 1107 cm) was retrieved approximately 1 km to the south-west of core SL6 (Figure 1c; 28.152250 °S; 32.519278 °E) in January 2012 using a vibrocorer. Core MF4-12 was sampled at a higher resolution than core SL6. Details with regard to the cataloguing, and sub-sampling are given in Baker et al. (2014, core SL6) and Miller et al. (2019, core MF4-12). Lithological description is also provided in detail therein. In brief, core SL6 varies between black to dark-brown fine-grained amorphous peat and includes occasional sandy lenses. Rootlets occur between 340-61 cm. Average core porosity is 0.7 and average bulk densities vary between 0.24 and 0.29 g cm^{-3} (Baker et al., 2014). Mass accumulation rates range between *c.* 21 and 103 g m^{-2} yr^{-1}, and total organic carbon contents range between *c.* 10 and 1600 g m^{-2} (Baker et al., 2014). As a result, carbon accumulation rates average 32 gC m^{-2} yr^{-1} during the

Holocene and 12 gC m^{-2} yr^{-1} over the remainder of the core (Baker et al., 2014). The Mfabeni peat lithology is heterogenous (Grundling et al., 2013) and the lithology of core MF4-12 differs from core SL6. In core MF4-12, the largest section (590-70 cm) contains peat with humus, fine detritus, and silt, while the upper section (70-0 cm) contains fibrous peat with humus and herbaceous fine detritus (Humphries et al., 2017; Miller et al., 2019). Grain sizes are largest (110 µm average) in the sandy peat section covering the Last Glacial Maximum (LGM) while smaller grains were deposited during the Holocene (50 µm average) (Humphries et al., 2017; Miller et al., 2019).

2.2. Radiocarbon dating and age model

Nine bulk peat samples from core SL6 and 24 samples from core MF4-12 were previously ^{14}C dated and calibrated using the Southern Hemisphere calibration curve, SHCal13, and post-bomb Southern Hemisphere curve, zones 1-2 (details in Baker et al., 2014; Miller et al., 2019). The AMS ^{14}C dates and the original age-depth models with uncertainty ranges are produced in Baker et al. (2014) for core SL6 and in Miller et al. (2019) for core MF4-12. In this study, the chronology was re-calibrated using SHCal20 (Hogg et al., 2020). The revised age-depth model is provided in Supplemental Information Figure S1. Age values were adjusted using the "rbacon" v 2.5.7 R package modelling software (Blaauw and Christen, 2011; Blaauw et al., 2020). The calibrated ages are herein referred to as thousand calibrated years BP and abbreviated as ka.

2.3. GDGT extraction and analysis

Core SL6: The core SL6 lipid biomarker extraction protocol was modified from Baker et al. (2016). Subsamples of 0.5 g freeze-dried material were extracted with 8 mL of 9:1 v/v dichloromethane:methanol (DCM:MeOH), agitated for 10 min, centrifuged and the supernatant pipetted into a new vial. The supernatant was centrifuged and reduced on a roto-evaporator. The total lipid extract was then re-eluted with 4 mL 9:1 v/v DCM:MeOH and filtered through Pasteur pipettes lined with glass wool and activated silica gel. The sample was evaporated to dryness and re-eluted using 1.5 mL of DCM:MeOH (9:1, v/v), which was then transferred to a 2 mL vial and evaporated to dryness under a gentle stream of high-grade nitrogen. The total lipid extract was re-dissolved in hexane/iso-propanol (99:1, v/v) and filtered using a 0.45 µm PTFE filter. The distribution of brGDGTs was analysed using high-performance liquid chromatography/atmospheric pressure chemical ionization – mass spectrometry (HPLC/APCI-MS) coupled to a ThermoFisher Scientific Accela Quantum Access triple quadrupole MS at the University of Bristol (Naafs et al., 2017). For normal phase separation, two ultra-high-performance liquid chromatography (UPLC) silica columns (Waters Acquity UHPLC HEB Hilic preceded by a guard column with the same packing) were used following Hopmans et al. (2016), resulting in the separation of the 5- and 6-methyl brGDGT isomers. An increase in sensitivity, as well as reproducibility of the sample peaks was achieved using the selective ion monitoring mode (SIM) and mass/charge (*m/z*) 1302, 1300, 1298, 1296, 1294, 1292, 1050, 1048, 1046, 1036, 1034, 1032, 1022, 1020, 1018, 744, and 653.

Core MF 4-12: Lipid biomarkers were extracted from freeze-dried and homogenized peat samples as described by Miller et al. (2019). In short, lipid biomarkers were extracted from *c.* 2 g peat with DCM:MeOH (9:1) using an Accelerated Solvent Extractor (ASE 200, DIONEX). The total lipid extract obtained was treated with copper turnings to remove elemental sulfur, dried under a gentle N_2 stream, and passed over a Na_2SO_4 column to remove water with hexane as eluent. The total lipid extract was saponified using 6% KOH in MeOH, back-extracted with hexane, and then passed over a silica gel column using hexane, DCM, and DCM:MeOH (1:1) to obtain a hydrocarbon, ketone, and polar fraction, respectively. Polar fractions were then re-dissolved in hexane:isopropanol (99:1) and filtered using a 0.45 µm PTFE filter. The brGDGTs were analyzed following the same procedure as for core SL6, except for using an Agilent 1260 Infinity UHPLC coupled to an Agilent 6130 single quadrupole mass detector at Utrecht University.

2.4. Proxy and air temperature calculation

In brief, the brGDGTs can vary in the amount and position of methyl branches as well as the number of cyclopentane rings (Weijers et al., 2007a; De Jonge et al., 2013). The degree of the methylation of the 5-methyl brGDGT isomers is related to temperature and quantified in the MBT'_{5me} index, while the number of cyclopentane moieties as well as the position of the methyl branches is related to pH, captured in the CBT index (Weijers et al., 2007a; De Jonge et al., 2014). The brGDGT distribution is used here to calculate the MBT'_{5me} index (De Jonge et al., 2014) following equation 1:

$$MBT_{5me}' = \frac{(Ia+Ib+Ic)}{(Ia+Ib+Ic+IIa+IIb+IIc+IIIa)} \qquad \text{(eq. 1)},$$

where Ia – Ic = tetra-, IIa – IIc = penta-, and IIIa = hexamethylated 5-methyl brGDGTs with 0-2 cyclopentane moieties.

The MBT'_{5me} index was converted to mean annual air temperature using the following peat-specific transfer function (Naafs et al., 2017):

$$MAAT_{peat}\ (^{o}\ C) = 52.18 \times MBT'_{5me} - 23.05 \qquad \text{(eq. 2)}.$$

The transfer function of Naafs et al. (2017) is based on the most comprehensive peat dataset that is currently available. Even though the majority of the peats in this dataset are from temperate regions, the temperature dependency of the brGDGTs appears consistent worldwide (Dearing Crampton-Flood et al., 2020; Raberg et al., 2022), corroborating the applicability of the transfer function based on this dependency in the subtropical Mfabeni peatland. Hereafter, we will refer to the $MAAT_{peat}$ as air temperature. The calibration error associated with $MAAT_{peat}$, i.e., the root mean square error, is 4.7 °C and is partly introduced by the spatial distribution and associated variability in environmental conditions of the investigated peats across the globe (Naafs et al., 2017). We infer here that when the proxy is applied downcore at any individual site, the error will be constant, and variations in MBT'_{5me}

can mostly be linked to (local) environmental changes. The analytical error on reconstructed temperatures is typically <0.5 °C based on repeated measurements of in-house standards.

In addition, we quantified the ratio of isoprenoid GDGT-0 (caldarchaeol) over crenarchaeol. This ratio likely reflects changes in temperature as well as in the archaeal community composition (Pearson and Ingalls, 2013). The ratio can indicate the presence of methanogenic archaea (Zhang et al., 2016). This assumption follows a simplified principle that Thaumarchaeota predominantly produce crenarchaeol, while GDGT-0 is also produced by Euryarchaeota, including methanogens (Turich et al., 2007; Schouten et al., 2013). Simplified, high GDGT-0 versus crenarchaeol ratios reflect oxygen depleted conditions and low ratios reflect oxygenated conditions (Zhang et al., 2016).

2.5. Stacked record

To provide a composite record from the two individual cores SL-6 and MF 4-12, we used Python Locally Weighted Scatterplot Smoothing (LOWESS) applying function "statsmodel.nonparametric.smoothers_lowess.lowess". In brief, this means fitting each point in the range of the dataset according to a weighted least square equation [(1 – |d|^3)^3], where d represents the distance of the respective points (i.e., observations/field data) to the point of estimation in the LOWESS curve fit. Thus, the further away the observations lie to the point of the curve being fitted, the less weight they have on the estimate (https://www.statsmodels.org/dev/generated/statsmodels.nonparametric.smoothers_lowess.lowess.html). The LOWESS-curve includes a smoothing parameter. For this, we used 10% of nearby data points for estimating the curve at each point in time, which means that the weighted least square equation only takes into account the closest 10 % of points.

To report uncertainties (confidence interval), we also calculated the LOWESS curves on bootstrapped data. The bootstrapping was made by first taking 100 random x-y-measurement pairs from the full population, calculating LOWESS-curve with same properties as used for the full dataset, and then repeating this procedure 100 times. For each x-value in the bootstrapping a mean and standard deviation of y was calculated, and from this 95% confidence intervals were calculated according to [mean ± 1.96*standard deviation]. This smoothing procedure does not incorporate age or proxy uncertainty.

3. Results

Stacked record: The composite record indicates major air temperature trends (Figure 2a). Air temperatures decreased by *c.* 5 °C across the late glacial period, from *c.* 20 °C at around 42.5 ka to a minimum temperature of *c.* 15 °C at *c.* 15.5 ka (Figure 2a). From this minimum, air temperatures increased, reaching 24.5 °C at the top of the core, representing the very latest Holocene (Figure 2a). The reconstructed average Holocene temperature is *c.* 20 °C. Shorter-scale climate fluctuations are also recorded, such as a major millennial-scale cooling event at *c.* 2.4 ka (Figure 2a).

Offsets between both cores: For most of the records, both cores show matching temperature trends that differ on average by *c.* 2 °C (Figure 2a), which is well within the 4.7 °C error associated with the global spatial $MAAT_{peat}$ calibration (Naafs et al., 2017). Over most of the late glacial period *c.* 28-15 ka, the SL6 core reflected consistently colder (Figure 2a) and wetter (Figure 2b-d) conditions compared to core MF4-12. Occasionally however, the difference between the two cores reaches *c.* 5-7 °C, especially at around 2.4 ka and 29 ka (Figure 2a). These differences are larger than the proxy error.

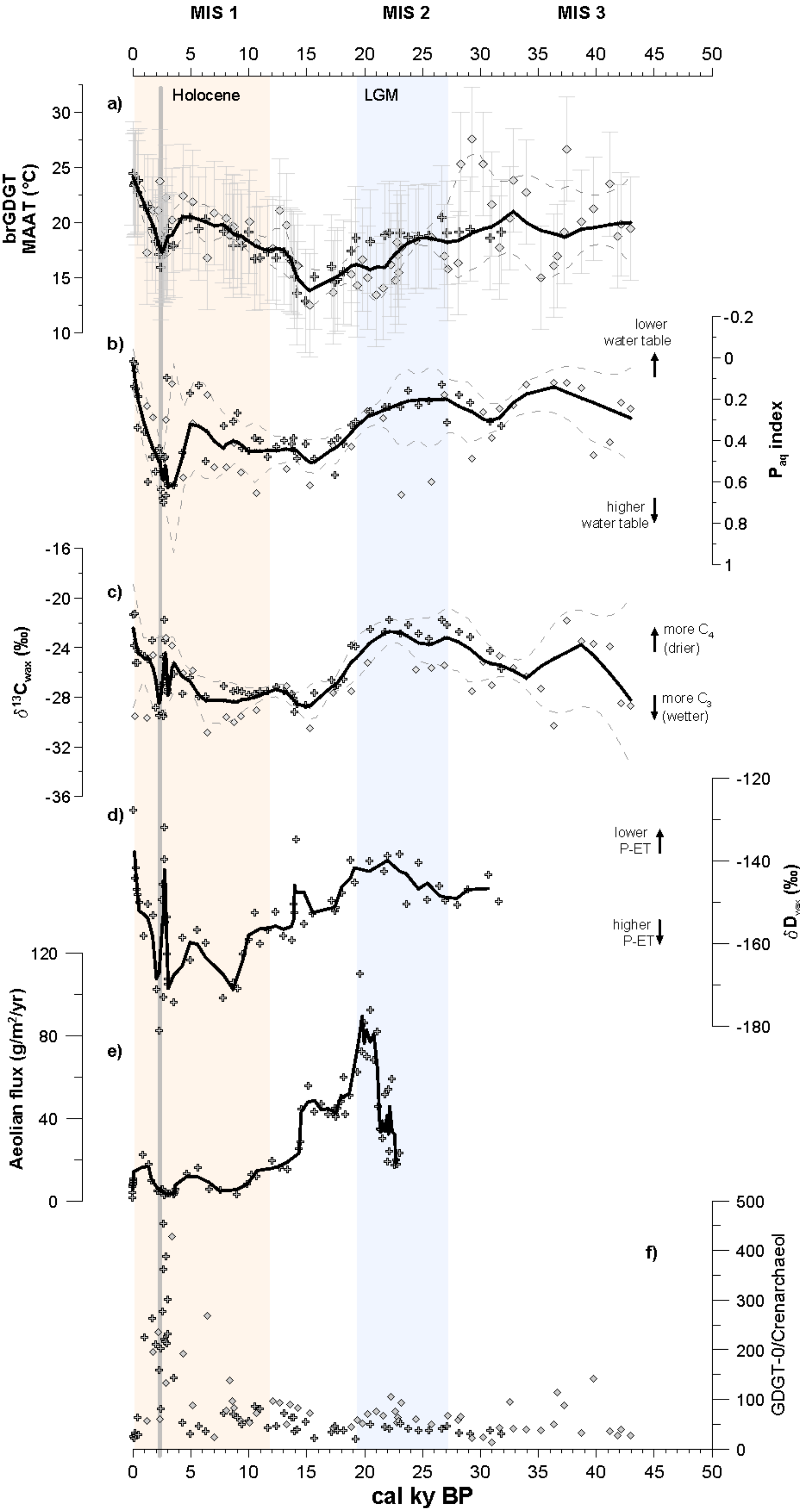
MIS 1
MIS 2
MIS 3
Holocene
LGM
a)
brGDGT MAAT (°C)
b)
lower water table
higher water table
P_{aq} index
c)
$\delta^{13}C_{wax}$ (‰)
more C_4 (drier)
more C_3 (wetter)
d)
lower P-ET
higher P-ET
δD_{wax} (‰)
e)
Aeolian flux (g/m^2/yr)
f)
GDGT-0/Crenarchaeol
cal ky BP

318

Figure 2*: Quantitative air temperature reconstructions from Mfabeni Peatland compared with previously published paleoenvironmental records from core sites SL6 (diamonds) and MF4-12 (crosses). (a) Branched glycerol dialkyl glycerol tetraethers (brGDGT) derived mean annual air temperatures (MAAT, this study). (b) Aquatic plant index (P_{aq}), where higher index values reflect more aquatic plants and lower values reflect more terrestrial plants (note the axis orientation; Baker et al., 2016; Miller et al., 2019). (c) Stable carbon isotope composition (weighted mean) of C_{29}–C_{31}* n-*alkanes ($\delta^{13}C_{wax}$) reflecting changes in C_3/C_4 vegetation (Baker et al., 2017; Miller et al., 2019). (d) Hydrogen isotope composition (weighted mean corrected for ice volume changes; Miller et al., 2019) of C_{29}–C_{31}* n-*alkanes (δD_{wax}), reflecting changes in precipitation amount and evapotranspiration (P-ET). (e) Aeolian flux (Humphries et al., 2017) reflecting changes in regional climate and wind. (f) Isoprenoid GDGT ratio GDGT-0 versus crenarchaeol that can be used as an indication of methanogenic archaea (this study). Simplified high GDGT-0/crenarchaeol ratios reflect oxygen depleted conditions and low ratios reflect oxygenated conditions. Grey error bars in panel a indicate calibration uncertainty (i.e., root mean square error of 4.7 °C) for each data point. Black lines in panels a-c represent LOWESS smoothed curves merging 0.1 fraction of data from cores SL6 and MF4-12. Dashed grey lines in panels a-c represent the upper and lower limits of the confidence interval. Lines in panels d-e represent 3-point running averages for core MF4-12.*

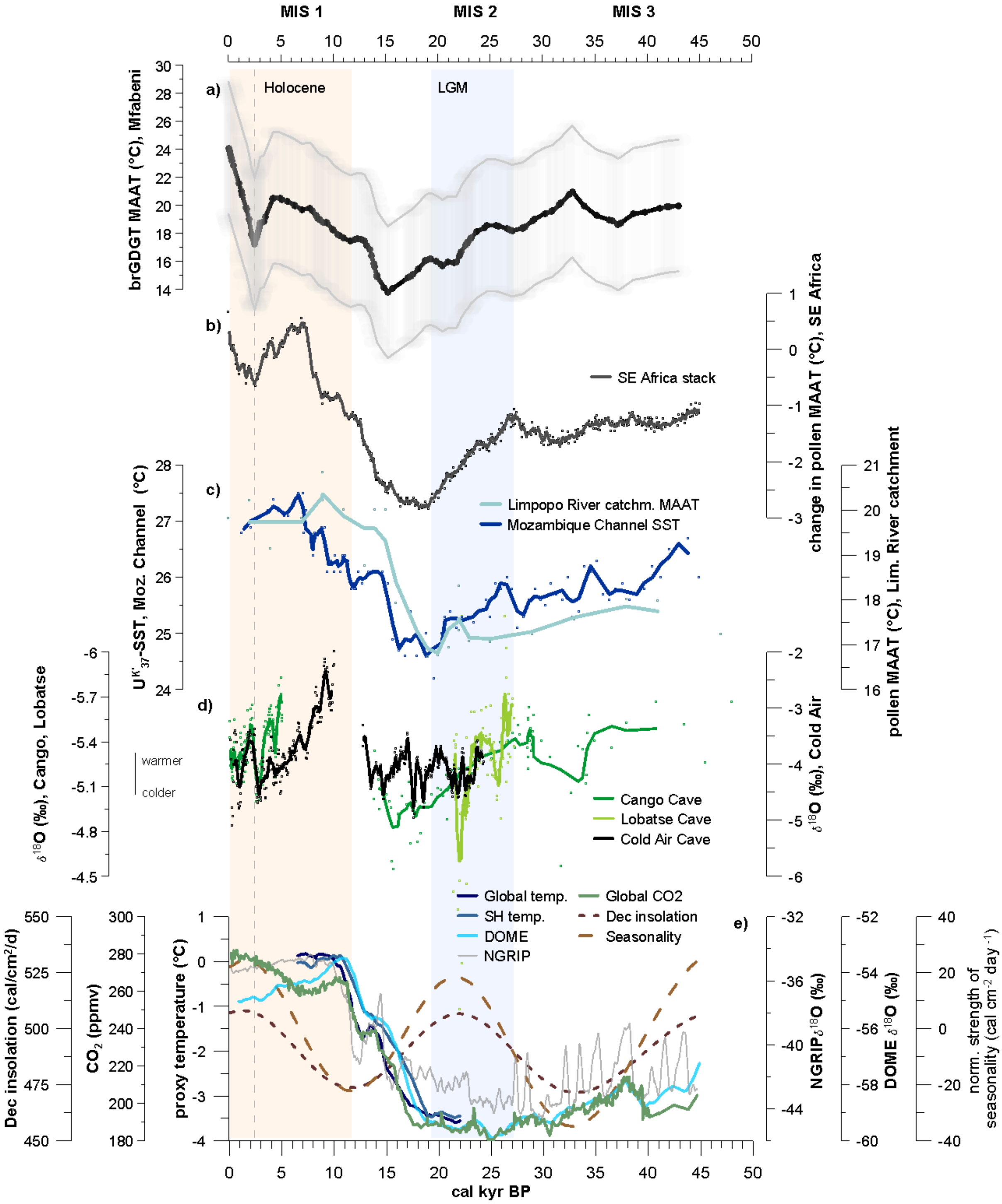

Figure 3: Quantitative air temperature reconstruction from Mfabeni Peatland (28.15 °S) (a) compared with published temperature records from southern Africa (b-d) as well as with hemispheric and global records (e). (a) Branched glycerol dialkyl glycerol tetraethers (brGDGT) derived mean annual air temperature (MAAT) from Mfabeni. The black line in panel a represents LOWESS smoothed curve merging data from cores SL6 and MF4-12 (cf. Figure 2a for both records). Grey lines and shades indicate calibration uncertainty. (b) Pollen-inferred MAAT stack record for south-eastern Africa (Chevalier and Chase, 2015). All lines in panels b-e represent 3-point running averages of the published data sets. Original

data points are displayed as circles in the respective colours. (c) Pollen-inferred MAAT from the Limpopo River mouth (light blue, Chevalier et al., 2020) and alkenone ($U_{37}^{K\prime}$)-derived sea surface temperatures (dark blue, SST) in the Mozambique Channel (Bard et al., 1997; Sonzogni et al., 1998; data access https://www.ncei.noaa.gov/access/paleo-search/study/9040). (d) $\delta^{18}O$ cave records from Lobatse Cave, Botswana (Holmgren et al., 1995, 1999), Cango Caves, south-western South Africa (Talma and Vogel, 1992), and Cold Air Cave, north-eastern South Africa (Holmgren et al., 2003); the $\delta^{18}O$-temperature relationship is adopted from the original papers (i.e., negative for Lobatse and Cango Caves, positive for Cold Air Cave). Note the axis orientation of the stalagmite and ice core $\delta^{18}O$ values in panels d and e. (e) $\delta^{18}O$ records from the North Greenland ice core (NGRIP; North Greenland Ice Core Project, 2004) and Antarctic DOME ice core (Kawamura et al., 2007), both lines represent 11-point running averages; Global CO_2 concentrations (48-22 ka: Ahn and Brook, 2014; 22-0 ka: Monnin et al., 2001); Global and southern Hemisphere multi-proxy temperatures (Shakun et al., 2012); December (summer) insolation at 30 °S (Berger and Loutre, 1991); Normalised strength of the seasonality, derived from subtracting winter (June) from summer (December) insolation at 30 °S (Berger and Loutre, 1991) normalised against mean insolation difference (following Darvill et al., 2016). Marine Isotope Stages (MIS 1-3) are indicated as defined by Lisiecki and Raymo (2005).

4. Discussion

4.1 Air temperature proxy record

The reconstructed Mfabeni air temperatures for the top of the stacked record (24.5 °C), as well as the data from the two individual cores (SL6: 23.4 °C and MF4-12: 24.7 °C), are higher than local contemporary mean annual air temperatures (*c.* 21.5 °C). They are, however, comparable with air temperatures of the warmest austral summer months (Jan-Mar; *c.* 24.5 °C) at this location (St. Lucia, https://climexp.knmi.nl/gettemp.cgi?WMO=68496). A bias towards summer temperatures has been observed in soils from locations with a strong seasonality in precipitation amount (e.g., under influence of the East Asian Summer Monsoon; Peterse et al., 2011; Deng et al., 2016; Wang et al., 2016), but does not occur in mineral soils from more temperate regions (e.g., Weijers et al., 2011b; Lei et al., 2016).

A bias towards summer temperatures in the aerated top of peat cores in mid/high-latitudes has been observed previously, but this bias disappears below the water table where the seasonal change in temperature is greatly reduced (Naafs et al., 2017). The datapoints derived from the upper 20 cm of the Mfabeni record are located above the depth of the modern water table (Clulow et al., 2012; Grundling et al., 2014) and may thus reflect summer temperatures. Since most of the brGDGT production in peats is assumed to take place around and below the water table (Weijers et al., 2004, 2006), where seasonal temperature variability is muted, the majority of our record will reflect mean annual temperatures. Hence, we here interpret the largest part of our $MAAT_{peat}$ record as corresponding to annual averages (cf. Naafs et al., 2017, and references therein).

It is, however, possible that seasonal and spatially distinct changes in the water table depth have introduced some scatter and slightly different trends between the two cores. For instance, lipid biomarkers in core SL6 recorded a relatively higher water table (P_{aq}; Figure 2b) and wetter conditions ($\delta^{13}C_{wax}$; Figure 2c) along with generally lower temperatures (Figure 2a) during the LGM and late last glacial compared to core MF4-12. This may have introduced a cold bias for core SL6 relative to core MF4-12. Also, core SL6 recorded an interval prior to 27 ka (Fig. 2a), with sub-orbital temperature oscillations of ~15 °C, well beyond the ~4 °C calibration uncertainty. This may partially be related to large variations in the water table (Fig. 2b). To compensate for the natural heterogeneity within the Mfabeni peatland, we will, therefore, focus on the composite annual air temperature record in the remainder of the discussion.

4.2 Mfabeni air temperatures from MIS 3 to LGM

Mfabeni annual air temperatures across MIS 3 average *c.* 20.5 °C (Figure 3a). That is *c.* 1 °C lower than modern instrumental annual air temperatures. This is consistent with the pollen-based Mfabeni and southern African stack MAATs (Chevalier and Chase, 2015) that also indicate *c.* 1 - 1.5 °C lower temperatures during MIS 3 compared to modern temperatures (Figure 3b). Pollen-based reconstructions from inland Wonderkrater boreholes show 1.5 to

2°C colder MIS 3 temperatures compared to modern temperatures (Chevalier and Chase, 2015).

Air temperatures decline from MIS 3 to MIS 2 and across the LGM, such that Mfabeni experienced more than 5°C cooling during this period with minimum temperatures of *c.* 15 °C (Figure 3a). As mentioned above, a much stronger cooling was observed in SL6 compared to MF4-12, especially between 23 and 20 ka, probably partially affected by local dynamics such as a higher water table and wetter conditions at the peat location of SL6 (Figure 2b,c). The brGDGT-based Mfabeni stacked temperature estimates follow a similar trend as the previously reconstructed annual temperature changes in south-east Africa based on pollen assemblages (Figure 3b), particularly at Mfabeni (Chevalier and Chase, 2015; Chevalier et al., 2020). However, the amplitude of cooling in the pollen-based MAAT records is less pronounced than that recorded by brGDGTs (Figure 3a,b), as pollen-based MAAT only declined by c. 2 °C at Mfabeni and in the south-east Africa stack (Chevalier and Chase, 2015). The larger amplitude in the Mfabeni brGDGT-based temperature record could be a result of a faster adaptation to temperature changes by brGDGT producing bacteria compared to vegetation, which is subject to inherent time lags as vegetation responds to prevailing climate. Moreover, the lack of temperature-sensitive pollen taxa linked to low taxonomic resolution in the pollen record creates a calibration problem at Mfabeni (Chevalier and Chase, 2015). It is, however, also possible, that other environmental constraints in and around Mfabeni prevent the vegetation from responding primarily to temperature changes. Still, the progressive cooling preceding the LGM at Mfabeni (Figure 3a) also matches major trends observed in the few available southern African speleothem $\delta^{18}O$ records (e.g., Figure 3d; Holmgren et al., 1995, 2003). The observed cooling trend is thus most likely a widespread southern African pattern, although the magnitude needs to be better constrained.

Local insolation cannot generally explain the observed changes in temperature at Mfabeni. However, the progressive decline in Mfabeni air temperatures during MIS 3 was concurrent to cooling in the south-western Indian Ocean, albeit more pronounced (Figure 3a,c). Lower water temperatures in the south-western Indian Ocean may have contributed to the decline in Mfabeni air temperatures, and at the same time also affected hydrological conditions (Baker et al., 2014, 2016, 2017; Miller et al. 2019; Finch and Hill, 2008; Grundling et al., 2013; Esteban et al., 2020). A potential scenario explaining lower temperatures in the south-western Indian Ocean is that Southern Ocean sea ice expansion and subsequent cooling (e.g., Bianchi and Gersonde, 2004) pushed the Southern Hemisphere westerlies further north (Hahn et al., 2021a). This northward displacement of the Southern Hemisphere westerlies caused a shift to drier and cooler conditions in the region, as also recorded by the intensification of the aeolian flux during the LGM (Figure 2e; Humphries et al., 2017). The more pronounced cooling at Mfabeni compared to the south-western Indian Ocean may thus arise from an amplification due to atmospheric circulation bringing colder air to the region. This could then also explain the observed cooling in other locations that are in the path of westerly-driven air masses, e.g. from the south coast passing by the interior in the few available $\delta^{18}O$ southern African speleothem records (e.g., Figure 3d; Holmgren et al., 1995, 2003).

4.3 Mfabeni air temperatures from LGM to Holocene

At the end of the last glacial, air temperature at Mfabeni increased by *c.* 5 °C. Although the timing is relatively similar (but see below), the magnitude of warming is higher than the *c.* 2.5 °C indicated by Chevalier and Chase (2015) using the south-east African pollen-based stack (Figure 3b). It is, however, close to the LGM-Holocene change of *c.* 4 °C indicated for some southern African sites, such as Wonderkrater (Truc et al., 2013) and Cango Caves (Figure 3d; Talma and Vogel, 1992). Climate models also indicate a 4-6 °C cooling in southern Africa during the LGM compared to modern-day (Engelbrecht et al., 2019). Furthermore, the brGDGT-based temperature change is within the range of previously published temperature changes in nearby terrestrial and marine records. For example, previous studies using $\delta^{18}O$ and noble gas concentrations in groundwater (Kulongoski et al., 2004), using pollen in sediments reflecting the Limpopo River catchment (Figure 3c; Chevalier et al., 2020), or using alkenones to estimate SST in the south-western Indian Ocean (Figure 3c; Bard et al., 1997; Sonzogni et al., 1998) indicate that LGM temperatures in and around southern Africa were *c.* 4-7 °C lower compared to modern-day.

The timing of the glacial/interglacial transition, i.e., the time when local temperatures increased in the Mfabeni peat, lagged that of the global CO_2 and temperature increase (Figure 3a,e), as well as the transition reflected by the south-east African pollen stack (Figure 3a,b) . The cooling slowed at Mfabeni at the end of the LGM at *c.* 20 ka and a brief, weak warming began, but this warming was interrupted by a return to cooler LGM-like conditions after *c.* 19 ka, such that the temperatures were lowest at *c.* 16-15 ka (Figure 3a). The warming towards Holocene temperatures at Mfabeni only resumed after *c.* 16-15 ka, corresponding to an increase in rainfall, water table, and relative abundance of C_3 vegetation (Figure 2a-d). In this context, a similar brief episode of warming at *c.* 17 ka followed by a return to cooling at *c.* 16 ka and resumed warming at *c.* 15 ka was also observed further north in Lake Chala in equatorial East Africa (Figure S2; Sinninghe Damste et al., 2012). Such cooling between 25 to 15 ka is however not reported in other temperature records representative of equatorial East Africa (e.g., Powers et al., 2005; Tierney et al., 2008; Loomis et al., 2017). However, the aeolian flux in the Mfabeni record also reflects that the shift to warmer and wetter conditions that began at the end of the LGM at *c.* 20 ka, was briefly interrupted and only resumed after *c.* 16-15 ka (Figure 2e; Humphries et al., 2017). This inference is consistent with the observations of delayed warming further inland, such as at Wonderkrater as illustrated in Chevalier and Chase (2015) and the return to colder conditions around 15 ka in the Cold Air Cave (Figure 3d; Holmgren et al., 2003). The Cango Caves also recorded a similar increase in temperatures only after *c.* 16-15 ka, during the Antarctic Cold Reversal, before a hiatus ensued until the middle Holocene, purportedly due to the poleward movement of the westerlies resulting in dry conditions (Figure 3d; Talma and Vogel, 1992). This brief interruption of the warming caused the apparent lag of the glacial/interglacial transition at Mfabeni compared to the global CO_2 and temperature evolution. The late warming matches the observations in air and sea surface temperatures in marine records east of southern Africa (e.g., the Mozambique Channel; Figure 3c) that began to increase only at *c.* 15.1 ka (Bard et al., 1997), reinforcing the assumption of the sea surface temperatures as primary control of late Quaternary south-east African air temperatures.

During the early Holocene, the Mfabeni brGDGT-based air temperatures indicate strong warming, similar to the pollen-based temperature stack (Figure 3a,b). During this period the Mfabeni peatland exhibits overall higher temperatures (Figure 2a), wetter conditions and higher water levels (Figure 2b-d), as well as a reduced aeolian input (Figure 2e; Humphries et al., 2017). However, at around 2.4 ka a period of marked cooling is evident at Mfabeni (Figure 2a). Although not present in global temperature stacks, this cool period is also apparent in the pollen-based temperature stack (Figure 3b; Chevalier and Chase, 2015). In addition, our two cores show relatively large temperature offsets at this time, pointing towards rapid, spatially heterogeneous responses within the peatland (Figure 2a). This short cold period is concurrent with rapid changes between higher/lower $\delta^{13}C_{wax}$ (Figure 2d) reflecting drier/wetter conditions, while P_{aq} indicates that the water table remained high (Figure 2b). Rapidly changing hydrological conditions are also indicated by a drastic increase in brGDGT concentrations (not shown) and in the ratio of isoprenoid GDGT-0 to crenarchaeol at around 2.4 ka (Figure 2f). BrGDGTs in peats are predominantly produced by (anaerobic) bacteria and their concentration is generally much higher in the water saturated and permanently anoxic part of a peat rather than in the oxic top section (Weijers et al., 2011b; Naafs et al., 2017). Hence, a drastic increase in brGDGT indicates water saturated conditions, i.e., a high water table. The GDGT-0 to crenarchaeol ratio can be used as a first order indication for the presence of methanogenic archaea versus ammonia oxidizing Thaumarchaeota, with a higher ratio under anoxic conditions due to the increase in methanogens (Blaga et al., 2009). The increase in GDGT-0/crenarchaeol ratio values in Mfabeni at 2.4 ka (Figure 2f) thus also indicates that anoxic conditions prevailed, likely resulting from changes in the water table depth.

In addition, Humphries et al. (2017) noted an increase in climate variability at Mfabeni during the late Holocene, with a short period of low aeolian deposition at *c.* 2.4 ka, which increased again after *c.* 2 ka (Figure 2e). Humphries et al. (2017) attributed the return to higher aeolian fluxes (i.e., drier conditions at Mfabeni) after *c.* 2 ka to a strengthened El Nino-Southern Oscillation (ENSO) activity. Geochemical evidence from nearby Lake Muzi and the Mkhuze Swamps provide additional evidence for pronounced hydroclimate variability during this period, which is also thought to reflect changes in ENSO activity (Humphries et al., 2019, 2020). Chase et al. (2017) noted this relatively abrupt, contrasting, inter-regional climatic evolution and attributed it to temperate and tropical influences on climatic interactions. The Mfabeni $MAAT_{peat}$ record confirms this period of climate instability around 2.4 ka. Nonetheless, air temperatures in the Mfabeni peat recovered after the 2.4 ka cooling period and steadily increased over the most recent c. 2 ka to reach close to modern-day (summer) temperatures (Figure 3a).

4.4 Mfabeni air temperatures during MIS3 and the Holocene

Global records indicate that MIS3 was milder and warmer than the preceding MIS 4 and the following MIS 2 in the Northern and Southern Hemispheres (e.g., Buizert and Schmittner, 2015), but not necessarily as warm as MIS5 or MIS1. In the brGDGT based Mfabeni temperature record, MIS 3 was as warm as the early Holocene (Figure 3a) and close to modern-day temperatures. The relatively high temperatures during MIS3 are not matched by temperatures derived from local pollen (Figure 3b) or global (Figure 3e) records, although speleothem data from further inland do suggest similarly high temperatures during MIS3 and MIS1 (Figure 3c). A relatively warm MIS 3 may have contributed to the initiation of the Mfabeni peatland, similar to peatland initiations in subtropical China at this time (Zhao et al., 2014). A lack of other contemporary brGDGT-based reconstructions from Southern Africa challenges corroboration of our warm, interglacial-like MIS 3 Mfabeni temperatures and requires further confirmation from future records.

In addition, MIS 3 is globally characterised by millennial-scale climatic changes (Siddall et al., 2008; Sanchez-Goñi et al. 2010). These rapid changes are potentially reflected in the SL6 record (Figure 2a), where brGDGT-derived temperatures vary in a range of more than 10 °C. However, the large amplitude of temperature change may partly be biased by the variations in hydroclimate and associated depth of the water table at that time (Figure 2b, c). Regardless, the temperature variability has largely been muted in the combined LOWESS smoothed stack (Figure 3a). Higher resolution climate reconstructions are needed to further constrain the magnitude and timing of (millennial) climatic changes at Mfabeni and to quantify the potential warm bias in the smoothed record.

5. Conclusion

To provide more insights into late Quaternary air temperature variability in south-east Africa and its sensitivity to global driving factors we generated a new continuous and quantitative air temperature record using brGDGTs lipids from Mfabeni peatland. The record covers the last 43 ka and suggests that atmospheric greenhouse gas concentrations and insolation are not a dominant control of local temperatures. This de-coupling between local temperatures and atmospheric greenhouse gases is especially clear during the deglaciation, but also implied by the high temperatures during MIS 3. We argue that this de-coupling is due to various oceanic and atmospheric heat transport processes, which implies that these processes are more important in this region than local radiative forcing.

Gradual cooling across MIS 3 was followed by an intensification of cooling during the LGM. The timing of the glacial/interglacial transition in the Mfabeni peat lagged the global CO_2 and temperature increase because of a brief return to colder and drier conditions after *c.* 19 ka. Deglacial warming began at around 16-15 ka in accordance with other records from southern Africa. The Holocene warm phase was briefly interrupted by a cooling event at *c.* 2.4 ka that is also evident in other records from the region, suggesting a regional impact. While the average Holocene temperatures of c. 20.0 °C were similar to those reconstructed for MIS 3, air temperatures in the Mfabeni peat steadily increased after the brief 2.4 ka cooling period, and reached close to modern-day summer temperatures of 24.5 °C at the top of the peat core. The overestimation of the annual modern-day temperatures of *c.* 21.5 °C in the top samples may be a result of a change in the heat capacity between aerated peat above, and the water saturated peat below the water table, leading towards a bias to summer temperature recorded by the brGDGTs at the top of the peat, which is consistent with other peat records. In summary, our record improves our understanding of south-east African quantitative air temperature evolution during the Late Quaternary and underlines the particular sensitivity and vulnerability of south-east Africa to global and regional climate forcings. We suggest that Mfabeni MAATs are affected, next to global changes, by Indian Ocean SSTs and position of the westerlies.

Acknowledgements

Patrick Prestele, Stellenbosch University, is acknowledged for support with SL6 sample processing. Ralph Kreutz, MARUM, is thanked for support with MF4-12 sample processing and analyses. David Rudberg, Linköping University, Linköping, Sweden, is acknowledged for support with Lowess smoothing. Figure 1 was drafted by Brice Gijsbertsen at the UKZN Geography Cartography Unit. This research has been supported by Stellenbosch University Sub-Committee-B Research Funding, National Research Foundation South Africa (Grant No: 98905, 84431), and Bundesministerium für Bildung und Forschung (BMBF; RAiN project, grant no. 03G0840A/B). Field work and other expenses were partly supported by a grant to J.R. from Ventenskapsrådet (Grant 348-2009-6500). B.D.A.N. was funded through a Royal Society Tata University Research Fellowship. F.P. acknowledges funding from the Nederlandse Organisatie voor Wetenschappelijk Onderzoek (NWO; Vidi grant 192.074). E.S. is supported by the DFG-Cluster of Excellence 'The Ocean in the Earth System' at MARUM. We thank Ezemvelo KZN Wildlife and iSimangaliso Wetland Park Authority for granting us permission to work at Mfabeni (OP 1630/2013). Three anonymous reviewers are acknowledged for valuable, insightful and respectful comments on this and previous versions that helped improve this manuscript.

Data availability

All data have been submitted to the Pangaea database [https://doi.pangaea.de/10.1594/PANGAEA.935696].

References

Baker, A., Pedentchouk, N., Routh, J., Roychoudhury, A.N., 2017. Climate variability in Mfabeni peatlands (South Africa) since the Late Pleistocene. Quaternary Science Reviews, 160, 57-66. https://doi.org/10.1016/j.quascirev.2017.02.009

Baker, A., Routh, J., Roychoudhury, A.N., 2018. *n*-Alkan-2-one biomarkers as a proxy for palaeoclimate reconstruction in the Mfabeni fen, South Africa. Organic Geochemistry, 120, 75–85. https://doi.org/10.1016/j.orggeochem.2018.03.001

Baker, A., Routh, J., Blaauw, M., Roychoudhury, A.N., 2014. Geochemical records of palaeoenvironmental controls on peat forming processes in the Mfabeni Peatland, Kwazulu Natal, South Africa since the Late Pleistocene. Palaeogeography, Palaeoclimatology, Palaeoecology, 395, 95-106. https://doi.org/10.1016/j.palaeo.2013.12.019

Baker, A., Routh, J., Roychoudhury, A.N., 2016. Biomarker records of palaeoenvironmental variations in subtropical southern Africa since the late Pleistocene: Evidences from a coastal peatland. Palaeogeography, Palaeoclimatology, Palaeoecology, 451, 1–12. https://doi.org/10.1016/j.palaeo.2016.03.011

Ballantyne, A.P., Greenwood, D.R., Sinninghe Damsté, J.S., Csank, A.Z., Eberle, J.J., Rybczynski, N. 2010. Significantly warmer Arctic surface temperatures during the Pliocene indicated by multiple independent proxies. Geology, 38, 603-606. 10.1130/G30815.1

Bard, E., Rostek, F., Sonzogni, C., 1997. Interhemispheric synchrony of the last deglaciation inferred from alkenone palaeothermometry. Nature, 385, 707-710. https://doi.org/10.1038/385707a0

Berger, A., Loutre, M.F., 1991. Insolation values for the climate of the last 10 million years. Quaternary Sciences Review, 10, 297-317. https://doi.org/10.1016/0277-3791(91)90033-Q

Bianchi, C., Gersonde, R., 2004. Climate evolution at the last deglaciation: the role of the southern Ocean, Earth Planet. Sc. Lett., 228, 407–424. https://doi.org/10.1016/j.epsl.2004.10.003

Blaauw, M., Christen, J.A., 2011. Flexible paleoclimate age-depth models using an autoregressive gamma process. Bayesian Analysis, 6, 457–474. https://doi.org/10.1214/11-BA618

Blaauw M, Christen JA, Aquino Lopez, MA, Vazquez, JE, Gonzalez, OM, Belding, T, Theiler, J, Gough, B, Karney, C (2020) Rbacon: age-depth modeling using Bayesian statistics. https://CRAN.R-project.org/package=rbacon

Blaga, C.I., Reichart, GJ., Heiri, O. Sinninghe Damsté, J.S., 2009. Tetraether membrane lipid distributions in water-column particulate matter and sediments: a study of 47 European lakes along a north–south transect. J. Paleolimnol., 41, 523–540. https://doi.org/10.1007/s10933-008-9242-2

Botha, G., Porat, N., 2007. Soil chronosequence development in dunes on the southeast African coastal plain, Maputaland, South Africa. Quaternary International, 162–163, 111–132. https://doi.org/10.1016/j.quaint.2006.10.028

Buizert, C., and A. Schmittner (2015), Southern Ocean control of glacial AMOC stability and Dansgaard Oeschger interstadial duration, Paleoceanography, 30, 1595–1612, doi:10.1002/2015PA002795

Caley, T., Extier, T., Collins, J.A., et al., 2018. A 2 million year-long hydroclimatic context for hominin evolution in southeastern Africa, Nature, 560, 76–79. https://doi.org/10.1038/s41586-018-0309-6

Carvalhais, N., Forkel, M., Khomik, M. et al. 2014. Global covariation of carbon turnover times with climate in terrestrial ecosystems. Nature 514, 213–217. https://doi.org/10.1038/nature13731

Chase, B.M., Meadows, M.E., 2007. Late Quaternary dynamics of southern Africa's winter rainfall zone. Earth-Science Reviews. 84, 103–138. https://doi.org/10.1016/j.earscirev.2007.06.002

Chase B.M., Meadows M.E., Carr, A.S., Reimer P.J. 2010. Evidence for progressive Holocene aridification in southern Africa recorded in Namibian hyrax middens: implications for African Monsoon dynamics and the 'African humid period'. Quaternary Research, 74, 36-45. https://doi.org/10.1016/j.yqres.2010.04.006

Chase, B.M., Lim, S., Chevalier, M., Boom, A., Carr, A.S., Meadows, M.E., Reimer, P.J., 2015a. Influence of tropical easterlies in the southwestern Cape of Africa during the Holocene. Quat. Sci. Rev. 107, 138e148.

Chase, B.M., Boom, A., Carr, A.S., Carré, M., Chevalier, M., Meadows, M.E., Pedro, J.B., Stager, J.C., Reimer, P.J., 2015b. Evolving southwest African response to abrupt deglacial North Atlantic climate change events. Quat. Sci. Rev. 121, 132e136.

Chase, B. M., Chevalier, M., Boom, A., Carr, A.S., 2017. The dynamic relationship between temperate and tropical circulation systems across South Africa since the last glacial maximum. Quaternary Sci. Rev., 174, 54–62. https://doi.org/10.1016/j.quascirev.2017.08.011

Chase B.M., Faith J.T., Mackay A., Chevalier M., Carr A.S., Boom A., Lim S., Reimer P.J., 2018. Climatic controls on Later Stone Age human adaptation in Africa's southern cape. J. Hum. Evol., 114, 35-44. https://doi.org/10.1016/j.jhevol.2017.09.006

Chase, B. M., Boom, A., Carr, A. S., Quick, L. J., Reimer, P. J. 2020. High-resolution record of Holocene climate change dynamics from southern Africa's temperate-tropical boundary, Baviaanskloof, South Africa, Palaeogeogr. Palaeocl., 539, 109518, https://doi.org/10.1016/j.palaeo.2019.109518.

Chevalier, M., Chase, B.M., 2015. Southeast African records reveal a coherent shift from high- to low-latitude forcing mechanisms along the east African margin across last glacial–interglacial transition, Quaternary Sci. Rev., 125, 117–130. https://doi.org/10.1016/j.quascirev.2015.07.009

Chevalier, M., Chase, B.M., Quick L.J., Dupont L., Johnson T.C., 2020, Temperature change in subtropical southeastern Africa during the past 790,000 yr. Geology, 49, 71–75, https://doi.org/10.1130/G47841.1

Clulow, A.D., Everson, C.S., Mengistu, M.G., Jarmain, C., Jewitt, G.P.W., Price, J.S., Grundling, P.L., 2012. Measurement and modelling of evaporation from a coastal wetland in Maputaland, South Africa. Hydrology Earth Systems Science, 16, 3233–3247. https://doi.org/10.5194/hess-16-3233-2012

Darvill C.M., Bentley M.J., Stokes C.R., Shulmeister J., 2016. The timing and cause of glacial advances in the southern mid-latitudes during the last glacial cycle based on a synthesis of exposure ages from Patagonia and New Zealand. Quat. Sci. Rev., 149, 200-214. https://doi.org/10.1016/j.quascirev.2016.07.024

Davis-Reddy, C.L., Vincent, K., 2017. Climate Risk and Vulnerability: A Handbook for Southern Africa (2nd Ed), CSIR, Pretoria, South Africa. http://hdl.handle.net/10204/10066

De Jonge C., Hopmans E.C., Stadnitskaia A., Rijpstra W.I.C., Hofland R., Tegelaar E., Sinninghe Damsté J.S., 2013. Identification of novel penta- and hexamethylated branched glycerol dialkyl glycerol tetraethers in peat using HPLC–MS2, GC–MS and GC–SMB-MS. Organic Geochemistry, 54, 78-82. 10.1016/j.orggeochem.2012.10.004

De Jonge, C., Hopmans, E.C., Zell, C.I., Kim, J.-H., Schouten, S., Sinninghe Damsté, J.S., 2014. Occurrence and abundance of 6-methyl branched glycerol dialkyl glycerol tetraethers in soils: implications for palaeoclimate reconstruction. Geochimica et Cosmochimica Acta 141, 97-112, doi: 10.1016/j.gca.2014.06.013

Dearing Crampton-Flood, E., Tierney, J.E., Peterse, F., Kirkels, F.M.S.A., Sinninghe Damsté, J.S.. 2020. BayMBT: a Bayesian calibration model for branched glycerol dialkyl glycerol tetraethers in soils and peats. Geochem. Cosmochim. Acta, 268, 142-159. https://doi.org/10.1016/j.gca.2019.09.043

Dupont, L.M. Caley, T., Kim, J.H., Castañeda, I.S., Malaizé, B., Giraudeau, J. 2011. Glacial–interglacial vegetation dynamics in South Eastern Africa coupled to sea surface temperature variations in the Western Indian Ocean. Clim. Past 7, 1209–1224. https://doi.org/10.5194/cp-7-1209-2011

Engelbrecht, F.A., Adegoke, J., Bopape M-J, Naidoo M, Garland R, Thatcher M., et al. 2015. Projections of rapidly rising surface temperatures over Africa under low mitigation. Environ. Res. Lett., 10, 085004. https://doi.org/10.1088/1748-9326/10/8/085004

Engelbrecht, F.A., Marean, C.W., Cowling, R.M., Engelbrecht, C., Nkoana, R., O'Neal, D., Fisher, E.C., Shook, E., Franklin, J., Neumann, F.H., Scott, L., Thatcher, M., McGregor, J.L., Van der Merwe, J., Dedekind, Z., Difford, M., 2019. Downscaling last glacial maximum climate over southern Africa. Quat. Sci. Rev., 226, 105879, 10.1016/j.quascirev.2019.105879

Esteban, I., Bamford, M.K., House, A., Miller, C.S., Neumann, F.H., Schefuß, E., Pargeter, J., Cawthra, H.C., Fisher, E.C., 2020. Coastal palaeoenvironments and hunter-gatherer plant-use at Waterfall Bluff rock shelter in Mpondoland (South Africa) from MIS 3 to the Early Holocene. Quaternary Science Reviews, 250, 106664. doi:10.1016/j.quascirev.2020.106664

Finch, J.M., Hill, T.R., 2008. A late Quaternary pollen sequence from Mfabeni Peatland, South Africa: reconstructing forest history in Maputaland. Quaternary Research 70, 442–450. https://doi.org/10.1016/j.yqres.2008.07.003

Gasse, F., Chalié, F., Vincens, A., Williams, M.A.J., Williamson, D. 2008. Climatic patterns in equatorial and southern Africa from 30,000 to 10,000 years ago reconstructed from terrestrial and near-shore proxy data. Quaternary Science Reviews, 27, 2316-2340. https://doi.org/10.1016/j.quascirev.2008.08.027

Grundling A.T., 2014. Remote sensing and biophysical monitoring of vegetation, terrain attributes and hydrology to map, characterise and classify wetlands of the Maputaland Coastal Plain, KwaZulu-Natal, South Africa. UWSpace. http://hdl.handle.net/10012/8457

Grundling, P., Clulow, A. D., Price, J. S., Everson, C. S., 2015. Quantifying the water balance of Mfabeni Mire (iSimangaliso Wetland Park, South Africa) to understand its importance, functioning and vulnerability. Mires and Peat, 16, 1–18. http://mires-and-peat.net/media/map16/map_16_12.pdf

Grundling, P.L., 2001. The Quaternary Peat Deposits of Maputaland, Northern KwaZulu-Natal, South Africa: Categorisation, Chronology and Utilisation. MSc thesis. University of Johannesburg. http://hdl.handle.net/10210/4303

Grundling, P.L., Grootjans, A.P., Price, J.S., Ellery, W.N., 2013. Development and persistence of an African mire: how the oldest South African fen has survived in a marginal climate. Catena 110, 176–183.

Gutiérrez, J.M., R.G. Jones, G.T. Narisma, L.M. Alves, M. Amjad, I.V. Gorodetskaya, M. Grose, N.A.B. Klutse, S. Krakovska, J. Li, D. Martínez-Castro, L.O. Mearns, S.H. Mernild, T. Ngo-Duc, B. van den Hurk, and J.-H. Yoon, 2021: Atlas. In Climate Change 2021: The Physical Science Basis. Contribution of Working Group I to the Sixth Assessment Report of the Intergovernmental Panel on Climate Change [Masson-Delmotte, V., P. Zhai, A. Pirani, S.L. Connors, C. Péan, S. Berger, N. Caud, Y. Chen, L.Goldfarb, M.I. Gomis, M. Huang, K. Leitzell, E. Lonnoy, J.B.R. Matthews, T.K.Maycock, T. Waterfield, O. Yelekçi, R. Yu, and B. Zhou (eds.)]. Cambridge University Press. In Press. Interactive Atlas. Available from http://interactive-atlas.ipcc.ch/

Hahn, A., Schefuß, E., Groeneveld, J., Miller, C., Zabel, M., 2021a. Glacial to interglacial climate variability in the southeastern African subtropics (25–20° S), Clim. Past, 17, 345–360, 2021a. https://doi.org/10.5194/cp-17-345-2021.

Hahn, A., Neumann F.H., Miller C., Finch J., Frankland T., Cawthra H.C., Schefuß E., Zabel, M. 2021b. Mid-to Late Holocene climatic and anthropogenic influences in Mpondoland, South Africa. Quaternary Science Reviews, 261, 106938.

Halamka, T.A., McFarlin, J.M., Younkin, A.D., Depoy, J., Dildar, N., Kopf, S.H. 2021. Oxygen limitation can trigger the production of branched GDGTs in culture. Geochem. Persp. Let. 19, 36–39.

Hogg, A., Heaton, T., Hua, Q., Palmer, J., Turney, C., Southon, J., et al. 2020. SHCal20 Southern Hemisphere Calibration, 0–55,000 Years cal BP. Radiocarbon, 62, 759-778. doi:10.1017/RDC.2020.59.

Holmgren, K, Paul, S. 1999. A Late Pleistocene Palaeoenvironmental Record from Lobatse II Cave. Botswana Notes and Records, 31, 73–81. www.jstor.org/stable/40980239.

Holmgren, K., Karlén, W., Shaw, P., 1995. Paleoclimatic Significance of the Stable Isotopic Composition and Petrology of a Late Pleistocene Stalagmite from Botswana. Quaternary Research, 43, 320-328. doi:10.1006/qres.1995.1038

Holmgren, K., Lee-Thorp, J.A., Cooper, G.R.J., Lundblad, K., Partridge, T.C., Scott, L., Sithaldeen, R., Talma, A.S., Tyson, P.D., 2003. Persistent millennial-scale climatic variability over the past 25,000 years in southern Africa. Quat. Sci. Rev. 22, 2311-2326. https://doi.org/10.1016/S0277-3791(03)00204-X

Holzkämper, S., Holmgren, K., Lee-Thorp, J., Talma, S., Mangini, A., Partridge, T., 2009. Late Pleistocene stalagmite growth in Wolkberg Cave, South Africa, Earth Planet. Sci. Lett., 282, 212– 221. https://doi.org/10.1016/j.epsl.2009.03.016.

Huber, M., Caballero, R., 2011. The early Eocene equable climate problem revisited. Climate of the Past 7, 603-633, doi: 10.5194/cp-7-603-2011

Humphries, M.S., Benitez-Nelson, C.R., Bizimis, M., Finch, J.M., 2017. An aeolian sediment reconstruction of regional wind intensity and links to larger scale climate variability since the last deglaciation from the east coast of southern Africa. Global and Planetary Change, 156, 59–67. https://doi.org/10.1016/j.gloplacha.2017.08.002

Humphries, M., Green, A., Higgs, C., Strachan, K., Hahn, A., Pillay, L., Zabel, M., 2020. High-resolution geochemical records of extreme drought in southeastern Africa during the past 7000 years. Quaternary Science Reviews, 236, 106294. https://doi.org/10.1016/j.quascirev.2020.106294

Humphries, M.S., Kirsten, K.L., McCarthy, T.S., 2019. Rapid changes in the hydroclimate of southeast Africa during the mid- to late-Holocene. Quaternary Science Reviews, 212, 178-186. https://doi.org/10.1016/j.quascirev.2019.04.006

Iturbide, M., Fernández, J., Gutiérrez, J.M., Bedia, J., Cimadevilla, E., Díez-Sierra, J., Manzanas, R., Casanueva, A., Baño-Medina, J., Milovac, J., Herrera, S., Cofiño, A.S., San Martín, D., García-Díez, M., Hauser, M., Huard, D., Yelekci, Ö. 2021. Repository supporting the implementation of FAIR principles in the IPCC-WG1 Atlas. Zenodo, DOI: 10.5281/zenodo.3691645. Available from: https://github.com/IPCC-WG1/Atlas

Johnson, T.C., Brown, E.T., McManus, J., Barry, S., Barker, P., Gasse, F., 2002. A high resolution paleoclimate record spanning the past 25,000 years in southern East Africa. Science, 296, 113–132. https://doi.org/10.1126/science.1070057

Kawamura K., Parrenin F., Lisiecki L., Uemura R., Vimeux F., Severinghaus J.P., Hutterli M.A., Nakazawa T., Aoki S., Jouzel J., Raymo M. E., Matsumoto K., Nakata H., Motoyama H., Fujita S., Goto-Azuma K., Fuji Y., Watanabe, O., 2004. Northern Hemisphere forcing of climatic cycles in Antarctica over the past 360,000 years. Nature, 448, 912–916. https://doi.org/10.1038/nature02805

Knight, J., Harrison, S., 2012. The impacts of climate change on terrestrial Earth surface systems. Nature Climate Change, 3, 24-29. https://doi.org/10.1038/nclimate1660

Kulongoski, J.T., Hilton, D.R., Selaolo, E.T., 2004. Climate variability in the Botswana Kalahari from the late Pleistocene to the present day. Geophys. Res. Lett., 31, L10204, doi:10.1029/2003GL019238.

Lappalainen, E., 1996. Global peat resources. International Peat Society. 359 p. Finland. ISBN 9529074875, 9789529074877

Lachniet, M.S., 2009. Climatic and environmental controls on speleothem oxygen-isotope values. Quatern. Sci. Rev., 28, 412–32. https://doi.org/10.1016/j.quascirev.2008.10.021.

Lei, Y., Yang, H., Dang, X., Zhao, S., Xie, S., 2016. Absence of a significant bias towards summer temperature in branched tetraether-based paleothermometer at two soil sites with contrasting temperature seasonality. Organic Geochemistry, 94, 83-94. https://doi.org/10.1016/j.orggeochem.2016.02.003

Lim, S., Chase, B.M., Chevalier, M., Reimer, P.J., 2016. 50,000 years of vegetation and climate change in the southern Namib Desert, Pella, South Africa. Palaeogeogr. Palaeoclimatol. Palaeoecol., 451, 197e209. https://doi.org/10.1016/j.palaeo.2016.03.001

Lisiecki, L. E., Raymo, M. E., 2005. A Pliocene-Pleistocene stack of 57 globally distributed benthic $\delta^{18}O$ records. Paleoceanography, 20, 1–17. https://doi.org/10.1029/2004PA001071

Loomis S.E., Russell J.M., Verschuren D., Morrill C., De Cort G., Sinninghe Damsté J.S., Olago D., Eggermont H., Street-Perrott F.A., Kelly M.A.. 2017. The tropical lapse rate steepened during the Last Glacial Maximum. Sci. Adv., 3. https://doi.org/10.1126/sciadv.1600815

Lukich, V., Cowling S, Chazan M., 2020. Palaeoenvironmental reconstruction of Kathu Pan, South Africa, based on sedimentological data. Quaternary Science Reviews, 230, 106153. https://doi.org/10.1016/j.quascirev.2019.106153

Lyons R., Tooth S., Duller, G.A., 2014. Late Quaternary climatic changes revealed by luminescence dating, mineral magnetism and diffuse reflectance spectroscopy of river terrace palaeosols: a new form of geoproxy data for the southern African interior. Quat. Sci. Rev., 95, 43-59. https://doi.org/10.1016/j.quascirev.2014.04.021

Meadows, M.E., Baxter, A.J., 2001 Holocene vegetation history and palaeoenvironments at Klaarfontein Springs, Western Cape, South Africa, Holocene, 11, 699–706. https://doi.org/10.1191/09596830195726

Meir, P., Cox, P., Grace, J., 2006. The influence of terrestrial ecosystems on climate. Trends in Ecology & Evolution 21, 254-260, doi: 10.1016/j.tree.2006.03.005

Miller, C., Finch, J., Hill, T., Peterse, F., Humphries, M., Zabel, M., Schefuß, E., 2019. Late Quaternary climate variability at Mfabeni peatland, eastern South Africa. Climate of the Past, 15, 1153–1170. https://doi.org/10.5194/cp-15-1153-2019

Miller, C., Hahn, A., Liebrand, D., Zabel, M., Schefuß, E., 2020. Mid- and low latitude effects on eastern South African rainfall over the Holocene, Quaternary Sci. Rev., 229, 106088, https://doi.org/10.1016/j.quascirev.2019.106088

Monnin, E., Indermühle, A., Dällenbach, A., Flückiger, J., Stauffer, B., Stocker, T.F., Barnola, J.M., 2001. Atmospheric CO_2 concentrations over the last glacial termination. Science, 291, 112–114. https://doi.org/10.1126/science.291.5501.112

Müller, J., Joos, F., 2020 Global peatland area and carbon dynamics from the Last Glacial Maximum to the present – a process-based model investigation, Biogeosciences, 17, 5285–5308, https://doi.org/10.5194/bg-17-5285-2020.

Naafs, B. D. A., Inglis, G. N., Zheng, Y., et al., 2017. Introducing global peat-specific temperature and pH calibrations based on brGDGT bacterial lipids. Geochimica et Cosmochimica Acta, 208, 285–301 https://doi.org/10.1016/j.gca.2017.01.038

Naafs, B.D.A., Inglis, G.N., Blewett, J., McClymont, E.L., Lauretano, V., Xie, S., Evershed, R.P., Pancost, R.D., 2019. The potential of biomarker proxies to trace climate, vegetation, and biogeochemical processes in peat: A review. Global and Planetary Change, 179, 57-79, doi: 10.1016/j.gloplacha.2019.05.006

Naafs, B.D.A., Oliveira, A.S.F., Mulholland, A.J. 2021. Molecular Dynamics Simulations Support the Hypothesis that the brGDGT Paleothermometer Is Based on Homeoviscous Adaptation. Geochim. Cosmochim. Acta 312, 44–56. doi:10.1016/j.gca.2021.07.034

Nash, D.J., Meadows, M.E., 2012. Africa, in: Metcalfe, S.E., Nash, D.J. (Eds.), Quaternary Environmental Change in the Tropics. John Wiley and Sons, Ltd., UK, pp. 79–150.

Neumann, F.H., Botha, G.A., Scott, L.2014. 18,000 years of grassland evolution in the summer rainfall region of South Africa: evidence from Mahwaqa Mountain, KwaZulu-Natal. Veget Hist Archaeobot 23, 665–681. https://doi.org/10.1007/s00334-014-0445-3

Partridge, T.C., P.B. DeMenocal, S.A. Lorentz, M.J. Paiker, Vogel J.C., 1997. Orbital forcing of climate over South Africa: a 200,000 year rainfall record from the Pretoria Saltpan. Quaternary Science Reviews, 16, 1125-1133. https://doi.org/10.1016/S0277-3791(97)00005-X

Pearson, A., Ingalls, A.E. 2013. Assessing the use of archaeal lipids as marine environmental proxies. Annual Review of Earth and Planetary Sciences 41, 359–384, https://doi.org/10.1146/annurev-earth-050212-123947.

Peterse, F., Prins, M.A., Beets, C. J., Troelstra, S.R., Zheng, H., Gu Z., Schouten, S., Sinninghe Damste, J.S., 2011. Decoupled warming and monsoon precipitation in East Asia over the last deglaciation. Earth Planet. Sc. Lett., 301, 256–264. https://doi.org/10.1016/j.epsl.2010.11.010

Peterse, F., van der Meer, J., Schouten, S., Weijers, J.W.H., Fierer, N., Jackson, R.B., Kim, J.H., Sinninghe Damsté, J.S., 2012. Revised calibration of the MBT–CBT paleotemperature proxy based on branched tetraether membrane lipids in surface soils. Geochim. Cosmochim. Acta, 96, 215–229. https://doi.org/10.1016/j.gca.2012.08.011

Porat, N., Botha, G., 2008. The luminescence chronology of dune development on the Maputaland coastal plain, southeast Africa. Quaternary Science Reviews, 27, 1024–1046. https://doi.org/10.1016/j.quascirev.2008.01.017

Powers, LA, Johnson, TC, Werne, JP. 2005. Large temperature variability in the southern African tropics since the Last Glacial Maximum. Geophysical Research Letters 32: L08706. https://doi.org/10.1029/2004GL022014

Raberg J.H., Miller G.H., Geirsdóttir Á., Sepúlveda J., 2022., Near-universal 126 trends in brGDGT lipid distributions in nature. Science Advances 8, eabm7625. https://doi.org/10.1126/sciadv.abm7625

Ramsay, P.J., Cooper, J.A.G., 2001. Late Quaternary Sea-Level Change in South Africa. Quaternary Research 57, 82-90. https://doi.org/10.1006/qres.2001.2290

Repinski, P., Holmgren, K., Lauritzen, S. E., Lee-Thorp, J.A, 1999. A late Holocene climate record from a stalagmite, Cold Air Cave, Northern Province, South Africa, Palaeogeogr. Palaeocl., 150, 269–277, https://doi.org/10.1016/s0031-0182(98)00223-5

Rydin, H. and Jeglum, J. K.. 2013. The Biology of Peatlands, 2nd edition, Oxford University Press, Oxford, 382 pp. https://doi.org/10.1093/acprof:osobl/9780199602995.001.0001

Sánchez Goñi, M.F., S.P. Harrison. 2010. Millennial-scale climate variability and vegetation changes during the last glacial: concepts and terminology. Quat. Sci. Rev., 29, 2823-2827. https://doi.org/10.1016/j.quascirev.2009.11.014

Schefuß, E., Kuhlmann, H., Mollenhauer, G., Prange, M., Pätzold, J., 2011. Forcing of wet phases in southeast Africa over the past 17,000 years. Nature, 480, 509-512. https://doi.org/10.1038/nature10685

Schmidt, F., Oberhänsli, H., Wilkes, H. 2014. Biocoenosis response to hydrological variability in Southern Africa during the last 84 ka BP: A study of lipid biomarkers and compound-specific stable carbon and hydrogen isotopes from the hypersaline Lake Tswaing, Global Planet. Change, 112, 92–104. https://doi.org/10.1016/j.gloplacha.2013.11.004

Schouten, S., Hopmans, E.C., Sinninghe Damsté, J.S., 2013. The organic geochemistry of glycerol dialkyl glycerol tetraether lipids: A review. Organic Geochemistry 54, 19-61. https://doi.org/10.1016/j.orggeochem.2012.09.006

Scott, L., Holmgren, K., Partridge, T.C., 2008. Reconciliation of vegetation and climatic interpretations of pollen profiles and other regional records from the last 60 thousand years in the Savanna Biome of southern Africa. Palaeogeography. Palaeoclimatology. Palaeoecology, 257, 198–206. https://doi.org/10.1016/j.palaeo.2007.10.018

Scott L, Neumann, F.H., 2018. Pollen-interpreted palaeoenvironments associated with the middle and late Pleistocene peopling of southern Africa. Quat. Int., 495, 169-184. https://doi.org/10.1016/j.quaint.2018.02.036

Scott L., Gil Romera, G., Marais, E. and Brook, G.A. 2018. Pollen in fossil hyrax dung from Marine Isotope Stages 2 and 3 reveals past environments in Namibia. Quaternary International, 464 A: 260-272. https://doi.org/10.1016/j.quaint.2017.06.054

Stager, J. C., Mayewski, P. A., White, J., Chase, B. M., Neumann, F. H., Meadows, M. E., King, C. D., and Dixon, D. A. 2012. Precipitation variability in the winter rainfall zone of South Africa during the last 1400 yr linked to the austral westerlies, Clim. Past, 8, 877–887. https://doi.org/10.5194/cp-8-877-2012

Seddon, A., Macias-Fauria, M., Long, P.R., Benz D., Willis K.J., 2016. Sensitivity of global terrestrial ecosystems to climate variability. Nature, 531, 229–232. https://doi.org/10.1038/nature16986

Siddall M., Rohling E.J., Thompson W.G., Waelbroeck C. 2008. Marine isotope stage 3 sea level fluctuations: Data synthesis and new outlook. Reviews of Geophysics, 46. doi: 10.1029/2007rg000226

Simon, M.H., Ziegler, M., Bosmans, J., Barker S., Reason C.J.C., Hall, I.R., 2015. Eastern South African hydroclimate over the past 270,000 years. Sci Rep, 5, 18153. https://doi.org/10.1038/srep18153

Sinninghe Damsté, J.S., Ossebaar, J., Schouten, S., Verschuren D., 2012. Distribution of tetraether lipids in the 25-ka sedimentary record of Lake Challa: extracting reliable TEX86 and MBT/CBT palaeotemperatures from an equatorial African lake. Quaternary Science Reviews, 50, 43-54, https://doi.org/10.1016/j.quascirev.2012.07.001

Sinninghe Damsté, J.S., Rijpstra, W.I.C., Foesel, B.U., et al., 2018. An overview of the occurrence of ether- and ester-linked iso-diabolic acid membrane lipids in microbial cultures of the Acidobacteria: Implications for brGDGT paleoproxies for temperature and pH. Organic Geochemistry, 124, 63-76, doi: 10.1016/j.orggeochem.2018.07.006

Singarayer J.S., Burrough S.L., 2015. Interhemispheric dynamics of the African rainbelt during the late Quaternary. Quat. Sci. Rev., 124, 48-67. https://doi.org/10.1016/j.quascirev.2015.06.021

Smuts, W.J., 1992. Peatlands of the natal mire complex - geomorphology and characterization. South African Journal of Science 88, 474–483. https://hdl.handle.net/10520/AJA00382353_9924

Sonzogni, C., Bard, E., Rostek, F., 1998. Tropical sea-surface temperatures during the last glacial period: A view based on alkenones in Indian Ocean sediments. Quaternary Science Reviews, 17, 1185–1201. https://doi.org/10.1016/S0277-3791(97)00099-1

Stevenson, C., Lee-Thorp, J. A., Holmgren, K, 1999. A 3000-year isotopic record from a stalagmite in Cold Air Cave, Makapansgat Valley, Northern Province. S. Afr. J. Sci., 95, 46–48. https://hdl.handle.net/10520/AJA00382353_7827

Talma, A.S., Vogel, J.C., 1992. Late quaternary paleotemperatures derived from a speleothem from Cango Caves, Cape Province, South Africa. Quat. Res., 37, 203-213. https://doi.org/10.1016/0033-5894(92)90082-T

Taylor, R., Adams, J.B., Haldorsen, S., 2006a. Primary habitats of the St Lucia Estuarine System, South Africa, and their responses to mouth management. African Journal of Aquatic Science, 31, 31–41. https://doi.org/10.2989/16085910609503869

Taylor, R., Kelbe, B., Haldorsen, S., Botha, G.A., Wejden, B., Været, L., Simonsen, M.B., 2006b. Groundwater-dependent ecology of the shoreline of the subtropical Lake St Lucia estuary. Environ. Geol., 49, 586-600. https://doi.org/10.1007/s00254-005-0095-y

Tierney, J.E., Russell J.M., Huang Y., Sinninghe Damsté J.S., Hopmans E.C., Cohen, A.S., 2008. Northern Hemisphere Controls on Tropical Southeast African Climate During the Past 60,000 Years. Science, 322, 252-255, doi: 10.1126/science.1160485

Truc, L., Chevalier, M., Favier, C., Cheddadi, R., Meadows, M.E., Scott, L., Carr, A.S., Smith, G.F., Chase, B.M., 2013. Quantification of climate change for the last 20,000 years from Wonderkrater, South Africa: implications for the long-term dynamics of the intertropical convergence zone. Palaeogeogr. Palaeoclimatol. Palaeoecol., 386, 575-587. https://doi.org/10.1016/j.palaeo.2013.06.024

Turich, C., Freeman, K.H., Bruns, M.A., Conte, M., Jones, A.D., Wakeham, S.G., 2007. Lipids of marine Archaea: Patterns and provenance in the water-column and sediments. Geochimica et Cosmochimica Acta, 71, 3272–3291. https://doi.org/10.1016/j.gca.2007.04.013

Venter, C.E., 2003: The vegetation ecology of Mfabeni peat swamp, St Lucia, KwaZulu-Natal. Unpublished MSc thesis. University of Pretoria, Pretoria. http://hdl.handle.net/2263/24480

Wang, H., Liu, W., Lu, H., 2016. Appraisal of branched glycerol dialkyl glycerol tetraether-based indices for North China. Org. Geochem., 98, 118–130. https://doi.org/10.1016/j.orggeochem.2016.05.013

Weijers, J.W.H., Schouten, S., van der Linden, M., van Geel, B., Sinninghe Damsté, J.S., 2004. Water table related variations in the abundance of intact archaeal membrane lipids in a Swedish peat bog. FEMS Microbiology Letters, 239, 51-56. doi: 10.1016/j.femsle.2004.08.012

Weijers, J.W.H., Schouten, S., Hopmans, E.C., Geenevasen, J.A.J., David, O.R.P., Coleman, J.M., Pancost, R.D., Sinninghe Damsté, J.S., 2006. Membrane lipids of mesophilic anaerobic bacteria thriving in peats have typical archaeal traits. Environmental Microbiology 8, 648-657, doi: 10.1111/j.1462-2920.2005.00941.x

Weijers, J.W.H., Schouten, S., van den Donker, J.C., Hopmans, E.C., Sinninghe Damsté, J.S., 2007a. Environmental controls on bacterial tetraether membrane lipid distribution in soils. Geochimica et Cosmochimica Acta, 71, 703–713. https://doi.org/10.1016/j.gca.2006.10.003

Weijers, J.W.H., Schefuß, E., Schouten, S., Sinninghe Damsté, J.S., 2007b. Coupled thermal and hydrological evolution of tropical Africa over the last deglaciation. Science, 315, 1701-1704. DOI: 10.1126/science.1138131

Weijers, J.W.H. Steinmann, P., Hopmans. E.C., Schouten, S., Sinninghe Damsté, J.S. 2011a. Bacterial tetraether membrane lipids in peat and coal: Testing the MBT-CBT temperature proxy for climate reconstruction. Org. Geochem., 42, 477-486.

Weijers, J.W.H., Bernhardt, B., Peterse, F., Werne, J.P., Dungait, J.A.J., Schouten, S., Sinninghe Damsté, J.S., 2011b. Absence of seasonal patterns in MBT–CBT indices in mid-latitude soils. Geochimica et Cosmochimica Acta, 75, 3179–3190. https://doi.org/10.1016/j.gca.2011.03.015

Yu, Z., Loisel, J., Brosseau, D. P., Beilman, D. W., Hunt, S. J. 2010. Global peatland dynamics since the Last Glacial Maximum, Geophys. Res. Lett., 37, 1–5, https://doi.org/10.1029/2010GL043584

Zhang, Z., Smittenberg, R., Bradley, R. 2016. GDGT distribution in a stratified lake and implications for the application of TEX_{86} in paleoenvironmental reconstructions. Sci Rep 6, 34465. https://doi.org/10.1038/srep34465

Zhao Y., Z.C. Yu, Y. Tang, H. Li, B. Yang, F.R. Li, W.W. Zhao, J.H. Sun, J.H. Chen, Q. Li, A.F. Zhou Peatland initiation and carbon accumulation in China over the last 50,000years Earth Sci. Rev., 128 (2014), 139-146. https://doi.org/10.1016/j.earscirev.2013.11.003

Zheng, Y., Li, Q., Wang, Z., Naafs, B.D.A., Yu, X., Pancost R.D., 2015. Peatland GDGT records of Holocene climatic and biogeochemical responses to the Asian Monsoon. Org. Geochem., 87, 86-95. https://doi.org/10.1016/j.orggeochem.2015.07.012

Zheng, Y., Pancost, R.D., Liu, X., et al., 2017. Atmospheric connections with the North Atlantic enhanced the deglacial warming in northeast China. Geology, 45, 1031-1034, https://doi.org/10.1130/G39401.1